Statistical Data Compression and Differential Coding for Digital Radio-Over-Fiber-Based Mobile Fronthaul

Mu Xu, Zhensheng Jia, Jing Wang, L. Alberto Campos, and Gee-Kung Chang

***Abstract*—Digital radio over fiber (D-RoF), one of the candidates for 5G mobile fronthaul networks, is known for its high reliability and strong robustness against nonlinear channel degradations, which makes it suitable for short-reach fronthaul links supporting ultra-reliable low-latency communication in 5G. However, traditional D-RoF technology is limited by its lower bandwidth efficiency. In this paper, based on our previous work, advanced data-compression techniques with adaptive non-uniform quantizers and differential coding are discussed for a significant improvement of bandwidth efficiency in fronthaul networks. High-order differential coding based on a least-mean-square algorithm has been proposed to further improve the compression ratio with low complexity and high adaptability. By jointly applying a non-uniform quantizer and a differentiator, the signal-to-quantization-noise ratio and bandwidth efficiency can be improved by around 10 dB and 40%–60%, respectively, depending on the modulation formats in our proposed solution. We have experimentally demonstrated the transmission of 200 Gbps fronthaul links over a fiber distance of 80 km. The system is capable of encapsulating 110 × 120 MHz 5G new radio carriers with error-vector magnitude lower than 0.8%.**

***Index Terms*—Digital radio over fiber; Mobile fronthaul; Optical fiber communication.**

I. Introduction

With the expectation of superior performance in throughput and connectivity, the fifth-generation new radio (5G-NR) air interface is going to be commercially launched around 2020 [1]. The new features of 5G, including higher-RF-band exploration, massive multiple input multiple output (MIMO), beam forming, ultra-reliable low-latency communication (uRLLC), and large-scale Internet-of-Things (IoT) connectivity, bring great challenges for next-generation mobile fronthaul (MFH) networks. Recently, both telecom industries and standard bodies have been working hard to finalize the design and specifications of the core network and radio access network (RAN) supporting 5G.

The centralized RAN (C-RAN) was proposed by China Mobile in 2011 [2]; here the baseband processing units (BBUs) are centralized and virtualized as a resource pool called the BBU pool, and its resources can be dynamically redistributed toward different radio access units on demand. While it has advantages in dealing with large-scale network resource allocation and data processing, the fully centralized architecture also leads to issues of high latency requirements and lack of flexibility. To address the issues and enhance the flexibility as well as compatibility with different application scenarios, C-RAN continues to evolve to accommodate new 5G RAN requirements and features. One of the new features is functional split (FS), which has been standardized on high layer split by 3GPP radio access architecture and interfaces release 14 [3]. In the 3GPP RAN architecture, two logical entities, namely, the central unit (CU) and the distributed unit (DU), are defined, and the functions in a traditional BBU can be divided between the CU and the DU in regard of radio resource control, packet data convergence protocol (PDCP), radio-link control (RLC), media access control (MAC), and physical (PHY) layers. There are eight options, which could realize a trade-off among radio performance, flexibility, delay, and transmission data rate.

Following the new requirements in 5G, the concept of next generation fronthaul interface (NGFI) has been proposed [4] to build an open and flexible platform supporting various services with diverse bandwidth and latency requirements. As illustrated by the conceptual diagram of NGFI in Fig. 1, two-layer fronthaul interfaces exist with Fronthaul-I connecting the DU and the remote radio unit (RRU) and Fronthaul-II connecting the CU and the DU. FS Option 2 with a split between PDCP and RLC has been adopted as the major option in Fronthaul-II. However, the FS option for Fronthaul-I is still open and it will depend on the service needs. As shown in Fig. 1, for the short-reach low-cost fronthaul system, two candidates in Option 8, namely, the analog radio over fiber (A-RoF) and the digital radio over fiber (D-RoF), are strong candidates to provide simple, robust, and low-latency data transmission links between the DU and the RRU, especially to fulfill the needs of massive machine-type communication, uRLLC, and vehicle-to-everything (V2X) communications.

Manuscript received July 11, 2018; revised September 18, 2018; accepted September 18, 2018; published October 22, 2018 (Doc. ID 338543).

M. Xu (e-mail: mxu35@gatech.edu), Z. Jia, J. Wang, and L. Alberto Campos are with CableLabs, Louisville, Colorado 80027, USA.

G.-K. Chang is with School of Electrical and Computer Engineering, Georgia Institute of Technology, Atlanta, Georgia 30332, USA.

https://doi.org/10.1364/JOCN.11.000A60

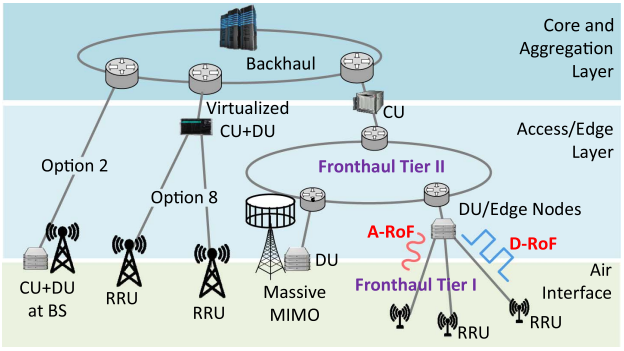

Fig. 1. Conceptual diagram of MFH architecture based on NGFI.

Fronthaul-I based on the A-RoF has been studied intensively [5–7]. Its benefits include high bandwidth efficiency and simple receiver architecture at the RRU. However, it also suffers from several major issues. First, the signals in the A-RoF are very sensitive to nonlinear degradations, channel penalties, and chromatic-dispersion-induced power fading. In order to guarantee the performance of the air-transmission link without disturbance from the optical systems, different nonlinear distortion-compensation techniques have been proposed [8–10] to compensate for the nonlinear distortions in the optical link. However, sophisticated digital signal processing (DSP) is required at the RRU site to restore the analog signals, thus greatly increasing the complexity. On the other hand, when multiple analog signals are aggregated in the frequency domain, complex analog subsystems or high-bandwidth analog-to-digital converters are needed to down-convert the signals from the intermediate frequencies. Moreover, the latest 5G-NR specifications feature filtered orthogonal frequency-division multiplexing (OFDM) and higher orders of modulations (256 and 1024-QAM) [11]. With the higher spectral efficiency, the upgrade of modulation in 5G also generates higher requirements on linearity and signal-to-noise ratio, where the shortcomings of the A-RoF seriously limit its signal quality and transmission distance.

Compared with the A-RoF, the D-RoF system digitizes and converts the continuous signal waveform to discrete voltage levels, which will be further degenerated to binary codes before modulation and transmission. Such techniques greatly improve the reliability and robustness of the system against different linear and nonlinear channel degradations. Moreover, the digitization process is straightforward, format-agnostic, and multiservice-compatible. Error-free transmission can also be achieved when employing forward-error correction (FEC) coding. Combined with efficient antenna-component (AxC) chip interleaving [12], point-to-multipoint efficient data multiplexing among antennas could also be realized. These features make the D-RoF technology a promising candidate for short-reach, highly reliable, and low-latency fronthaul links supporting IoT, machine-type, and V2X communications in 5G.

One of the major problems regarding the D-RoF stems from its low bandwidth efficiency in transmission. The common public radio interface (CPRI) has been widely used in current MFH supporting long-term evolution (LTE). To transmit one 20 MHz LTE component, with 15-digit quantization, 1-digit control word, and 8b/10b encoding, a capacity of nearly 1.2 Gbps is required in the fiber link, which is inefficient. Fortunately, multiple solutions, including resampling, data compression, and advanced modulation formats, could help to increase the bandwidth efficiency of D-RoF systems. Among them, data compression is the key study item of this paper. A lot of work has been done in this area, including partial-bit sampling (PBS) [13], nonlinear quantization [14,15], statistical estimation [16,17], vector quantization [18], and differential pulse-code modulation (DPCM) [19]. Great achievements have been reported where, depending on the signal-to-quantization-noise (SQNR) threshold, almost 50% bandwidth can be saved [20]. The requirement of digital-to-analog-converter (DAC) resolution is also relaxed, which approaches that of transmitting symbols before inversed fast-Fourier transform (IFFT) in the PHY-I-split option. In the following part of the paper, it is demonstrated that by applying the adaptive statistical algorithm and integrating the quantizer and differential encoder into a feedback-loop-based architecture, the bandwidth efficiency can be further improved by more than 60%, with a 10 dB improvement in SQNR. In the meantime, the applicable waveform has been expanded from OFDM to other frequently used wireless formats, like single-carrier frequency-division multiplexing (SC-FDM). Sufficient system margin from the threshold can be obtained. Since data compression is widely studied and is under discussion among standard bodies [15,21] as well as hardware vendors [22], the results of the work could potentially pave the way for future development in this area.

Recently, multiple FS options in 3GPP RAN architecture [3], NGFI [4], and eCPRI [21] have been actively discussed. With FS, especially a deep split at the MAC and RLC layers, fronthaul data can be multiplexed over Ethernet packets and the required bandwidth is expected to be greatly reduced. However, there are still a lot of issues. First of all, the reduction of bandwidth is at the expense of higher complexity and cost of the DU, especially when dealing with MIMO processing and coordinated multipoint transmission. Second, the DU may need to change the FS options adaptively or enable multiple FS options to coexist to support different using scenarios, which also greatly increases the complexity. Moreover, FS is not exclusive to the D-RoF technology. In some FS options, like PHY-I or I_D split [23], quantization is still needed to digitally convert the symbols after MIMO precoding.

The paper is organized as follows: in Section I, we provide the background and motivations of the study. Section II summarizes the existing work and our contributions. In Section III, we explain the operation principle of the adaptive statistical method in non-uniform quantizer (NUQ) design. Section IV demonstrates the high-order DPCM encoder and decoder enhanced by the least-mean-square (LMS) algorithm. Section V shows some selected experimental results. Finally, we conclude the paper in Section VI.

II. Related Works and Our Contributions

Before starting the technical discussions, it is important to understand the role of data compression in future digital MFH systems. The flow diagrams of functions in MFH with data compression are shown in Fig. 2. In the transmitter part of the D-RoF, the operation is initiated from complex-valued analog carriers. For each analog signal sample of the component carrier (CC), the in-phase (I) and quadrature (Q) parts are separated, where the continuously varied amplitudes will be quantized into discrete samples, with 2^U quantization levels for each sample. Then linear pulse-code modulation (PCM) or DPCM is applied to convert the quantization levels into U-bit binary codes, which is also called an AxC chip. After that, certain compression algorithms are used to reduce the size of each AxC chip. Through a training process, each U-bit chip can be mapped into V bits and, in this case, the required bandwidth can be reduced by a factor of $(U-V)/V$. D-RoF frames are formed by interleaving different AxC chips for different antennas in the time domain. Then, different combinations of FEC line coding and modulation formats are applied. In the receiver site of the D-RoF, the procedures are reversed, where demodulation, FEC decoding, and de-framing are performed subsequently. After the AxC chips are recovered, the inverse bit map will be applied to map each chip from V bits back to U bits. It is worth noting that the inverse bit map is generated by reversing the bit-mapping input and output obtained by the compressor at the transmitter site, which will be transported to the receiver site as part of the system control information in the overhead. After the DPCM/PCM decoder and the DAC, the discrete level of each sample is reconstructed from the bits and the analog waveform is re-generated, which is ready for the air transmission. It can be noted that the critical procedures of the data compressor are mainly performed at the transmitter site and, apart from the data channel, a control channel is also needed to control, manage, and coordinate the operation of data compression between the transmitter and receiver sites.

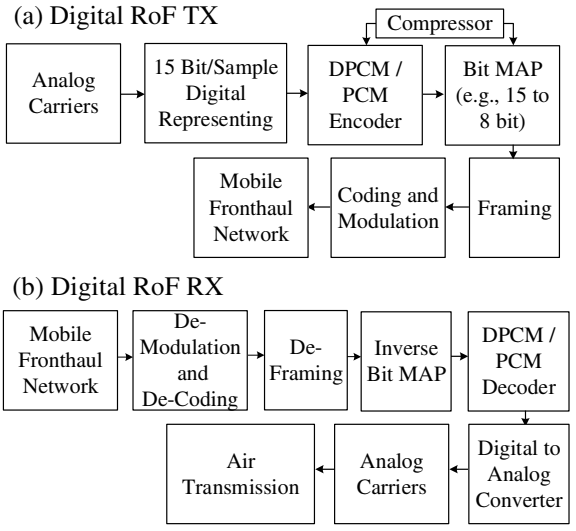

Fig. 2. Signal processing procedures in MFH with data compression in (a) DL and (b) UL transmissions.

Different data compression algorithms have been proposed. Among these, PBS proposed by ETRI [13] is simple to implement. In PBS, for a U -to-V-digit compression, the last $(U-V)$ digits are directly cut off, which is equivalent to a V-digit uniform quantization process. But this hard truncation results in large quantization noise when reducing the number of digits. Fitting-based nonlinear quantization is recommended by the Open Radio Equipment Interface [15]. It is based on the Gaussian distribution nature of the OFDM signal's amplitudes, thus obtaining improved accuracy. However, the algorithm requires estimating the statistical properties of the Gaussian distribution from a large number of training samples, which is time consuming and may not be applicable to non-Gaussian wireless formats.

To simplify the computationally complex fitting process and in the meantime guarantee signal quality after compression, fast-statistical estimation or K-Law has been proposed [17,24]. K-Law is also based on the Gaussian distribution property of OFDM signals and assumes that the Gaussian function can be truncated within the range of $[-K\sigma \quad K\sigma]$, where σ is the standard variance and K is an adjustable positive number. Recall that more than 99.6% amplitudes are distributed within $[-3\sigma \quad 3\sigma]$. So, by setting a K value around 2.5–3, high accuracy can be obtained in K-Law. After taking the absolute value and performing normalization to each D-RoF data block, σ can be immediately obtained from the relation $x_{\max} = K\sigma = 1$ and it will be used to build the companding transform function $y = C(x)$. The companding function is used to linearize the cumulative distribution function of the signal's amplitude. After that, uniform quantization is applied to the companded signals and the quantization noise becomes nearly uniform within each quantization section. According to the minimum mean-square-error (MMSE) criterion, the overall quantization noise is minimized, which allows us to use fewer number of quantization digits to generate each AxC chip. The error-vector magnitude (EVM) after K-Law-based 15-to-8-digit compression and de-compression processes could reach around 0.6%.

However, one major drawback of the K-Law method is that it is based on the assumption of a Gaussian distribution. However, a lot of wireless formats, like SC-FDM and Nyquist pulsed single-carrier modulation, do not strictly follow a Gaussian distribution. Under these circumstances, the accuracy of K-Law is significantly degraded. Some traditional general-purpose companding methods, such as μ-Law and A-Law, may outperform K-Law in regards to non-Gaussian distributed waveforms. In what follows, it has been demonstrated that the adaptive statistical method with the Lloyd algorithm could theoretically process any kind of formats while obtaining a good signal quality.

Recently, machine-learning-enhanced multi-dimensional quantization (MDQ) was also proposed in Ref. [18]. The traditional methods mentioned before perform quantization and data compression in the real scalar domain toward

either the I or Q component. However, in MDQ, first an N-dimensional vector group is constructed based on the original samples. Then, an N-dimensional K-means clustering algorithm is applied to slice the vector space into M clusters, while data falling inside each cluster will be allocated a quantization codeword. It has been demonstrated that significant improvement in the performance of EVM can be obtained through the proposed 2D and 3D quantization. Nevertheless, the major drawback of this method stems from its high complexity. For a 15-to-8-digit compression, the proposed method needs to calculate 2^{16} clusters in 2D quantization, which is challenging to apply in a practical low-latency MFH system.

The methods introduced above are concerned with the design of quantizers in a PCM system. Another important research direction in this area is DPCM [19,25]; it can also be used to suppress the quantization noise level, and when it jointly works with new quantizers, significant performance enhancement can be achieved. The basic idea of DPCM is based on the fact that most source signals exhibit some correlations between successive samples, which can result from over-sampling, presenting of long-ones/zeros, or certain coding techniques; through differential precoding, the correlation-induced redundancy can be reduced, which enables representing the information with fewer digits. Given the original analog waveform samples, $x(k)$, and the reconstructed waveform samples after the compression–decompression process, $x_q(k)$, the idea of Nth-order DPCM is to quantize the error sequence of the weighted differentiated samples instead of the original samples, which is denoted as

$$\mathrm{err}(k) = x(k) - \hat{x}(k), \tag{1}$$

$$\hat{x}(k) = \sum_{i=1}^{N} c_i x_q(k-i), \tag{2}$$

where $\hat{x}(k)$ is also called the prediction symbol of $x(k)$. According to the Wiener theory [26], the best weight coefficients of $c_i|_{i=1\sim N}$ can be obtained by minimizing the mean-square error (MSE), $J = E[|\mathrm{err}(k)|^2]$. It has been reported in Ref. [19] that by applying fourth-order DPCM plus a nine-digit uniform quantizer, less than 0.5% EVM can be achieved. However, to determine the optimal coefficients, the traditional MMSE-based method requires building the correlation matrix from a lot of training data, and solve the inverse of it, which is computationally inefficient and lacks the flexibility to process the dynamically varied wireless signals.

In this paper, we have further studied the design and operation of a joint architecture of NUQ and a differentiator. Compared with our work in Ref. [16], improvements are made in two aspects. Above all, more details are provided about the relaxed Lloyd (R-Lloyd) algorithm based on our previous results in Ref. [16]. Mechanisms for suppressing the quantization noise, thus improving the bandwidth efficiency in D-RoF MFH, have been analyzed theoretically. On the other hand, a DPCM-NUQ joint compressor is employed to further improve the bandwidth efficiency, and we propose using a LMS-algorithm-based adaptive filter to determine the values of the weights toward the high-order differential encoder. Compared with existing methods, the LMS-based DPCM is computationally more efficient, with high accuracy and adaptability. High signal quality after de-compression has also been achieved through the experimental demonstrations.

R-Lloyd-algorithm-based MFH with data compression has been demonstrated in this paper; this can support 1024-QAM in the latest 3GPP specifications and a future-proof 4096-QAM format. To reduce the complexity, the traditional Lloyd algorithm is applied to calculate the major quantization levels and the minor quantization levels are uniformly interpolated between two adjacent major levels. The selection of the number of major and minor levels results in a trade-off between computational complexity and signal quality. Compared with existing methods such as K-Law, μ-Law, and A-Law [27], the quantization noise can be reduced by around 4.8 dB. Different from statistical estimation methods like K-Law, the Lloyd algorithm is format-agnostic and applicable to non-Gaussian modulation formats, like SC-FDM.

Adaptive DPCM based on LMS has also been proposed in this paper. Compared with the existing MMSE algorithm, it shows no significant sacrifice of performance accuracy. Also, it adds two benefits: first, the computational complexity is greatly reduced especially when calculating the coefficients for the high-order differentiator. Second, the algorithm is based on an adaptive filter architecture; the weights of the taps in a differentiator can be adaptively adjusted according to the statistical property of the waveform at different times. The performance of the LMS method has been confirmed by comparing it with the look-up-table (LUT) [28] method, which finds the global optimized tap coefficients of the differentiator through hard searching all possible combinations of tap coefficients in a certain range. The similar performance of the two proves the effectiveness of the LMS method. It is also confirmed that the SQNR improves when applying a higher-order differentiator. However, the gain margin also diminishes under the higher-order differentiator. Considering the complexity and performance, a good trade-off can be obtained with a third- or fourth-order differentiator. Through the simulation and experimental results, after combining R-Lloyd and DPCM, SQNR improvements of around 6, 8, and 10 dB can be obtained at the first, second, and fourth-order differentiators, respectively.

The proposed technology is also demonstrated experimentally over 180 Gbit/s QPSK and 200 Gbit/s 16-QAM coherent optical fronthaul systems. Considering a subcarrier separation of 60 kHz, and a sampling rate of around 120 MHz for each 5G-NR CC, a 200 Gbit/s system could encapsulate 90 or 110 carriers with the 1024-QAM format under 15-to-8-bit or 15-to-7-bit compression, respectively. The compression performance under the influence of bit errors is also measured and the EVM degradation by using DPCM instead of PCM is insignificant and so such influence could be mitigated by employing FEC coding.

III. Operation Principle and Performance Evaluation of the Relaxed Lloyd Algorithm

The operation principle and procedures of the R-Lloyd algorithm are shown in Fig. 3. Given the modulus (absolute value) of the signal, $x = |s|$, the Lloyd algorithm starts with the probability distribution function (PDF) of x before compression, $f(x)$, as shown in Fig. 3(a). It first divides x into $N = 2^V$ quantization segments and each of the segments is bounded with two quantization thresholds, from Segment 1 with t_1 and t_2, until Segment N with t_N and t_{N+1}. N quantization levels from l_1 to l_N are allocated for Segment 1 to Segment N, respectively. Thus, there are in total N quantization levels and $N + 1$ thresholds. For the samples falling into Segment i, they will be quantized into l_i.

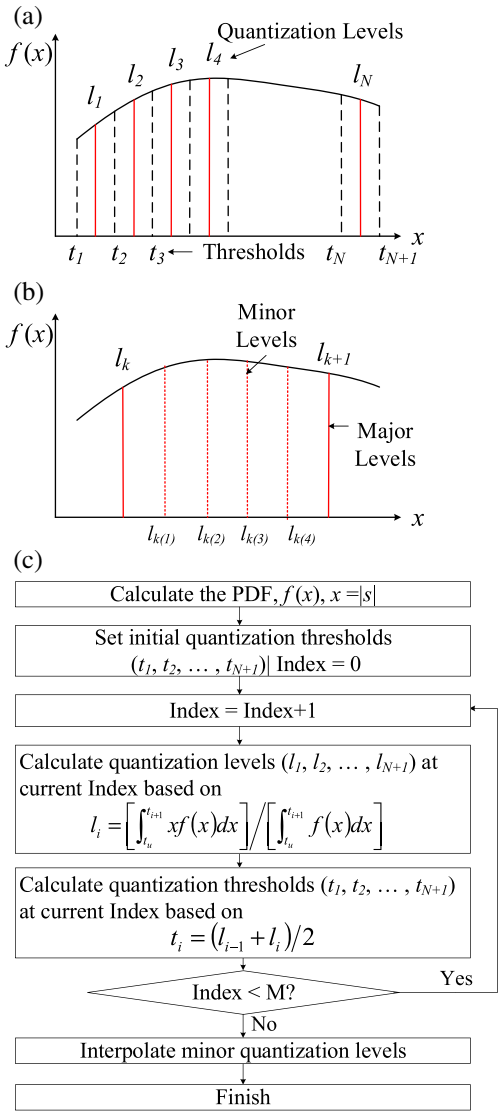

Fig. 3. (a), (b) Operation principles of Lloyd and relaxed-Lloyd algorithms. (c) Flow diagram of the quantization process using R-Lloyd algorithm.

Let two random variables X and X_q denote, respectively, the signal's modulus before and after quantization. Given l_1 to l_N and t_1 to t_{N+1}, the objective of the Lloyd algorithm is to minimize the MSE between X and X_q, which can be calculated as

$$e^2_{\mathrm{MSE},Q} = E[(X_q - X)^2]. \tag{3}$$

When $f(x)$ is known, Eq. (3) can be rewritten as

$$e^2_{\mathrm{MSE},Q} = \sum_{i=1}^{N} \int_{t_i}^{t_{i+1}} (l_i - x)^2 f(x)\mathrm{d}x. \tag{4}$$

The minimum MSE value must appear at the extreme points on the surface of $e^2_{\mathrm{MSE},Q}$, which can be expressed by

$$\frac{\partial(e^2_{\mathrm{MSE},Q})}{\partial t_i} = 0, \qquad i = 1, 2, \ldots, N+1, \tag{5}$$

$$\frac{\partial(e^2_{\mathrm{MSE},Q})}{\partial l_i} = 0, \qquad i = 1, 2, 3, \ldots, N. \tag{6}$$

Combining Eqs. (4)–(6), the following relations can be obtained:

$$t_i = (l_{i-1} + l_i)/2, \qquad i = 2, 3, \ldots, N, \tag{7}$$

$$l_i = \int_{t_i}^{t_{i+1}} x f(x)\mathrm{d}x \Big/ \int_{t_i}^{t_{i+1}} f(x)\mathrm{d}x, \qquad i = 1, 2, \ldots, N. \tag{8}$$

It is Eqs. (7) and (8) that build the foundation of the Lloyd algorithm, with the flow diagram shown in Fig. 3(c). The first step in the Lloyd algorithm is to initialize the quantization thresholds and levels. It is worth mentioning that, typically, a data-compression algorithm is executed over data blocks. For each data block, after removing the DC component and normalizing the modulus into the range of [0 1], a simple rule to determine the initial first and last values of thresholds are $t_1 = 0$ and $t_{N+1} = 1$. Then, t_2 to t_N can be uniformly inserted from 0 to 1 and the initial values of l_1 to l_N can be calculated using Eq. (8). After initialization, the Lloyd algorithm will take iterations to calculate the quantization thresholds from previous values of levels using Eq. (7), and the quantization levels are calculated from former thresholds based on Eq. (8) until the MSE converges to a certain value or the iteration index meets its maximum. Supposing each original OFDM sample at the transmitter is represented as a U-digit code and each output quantization level is denoted with a V-digit code ($V = \log_2 N$), based on the final output of the compressor, U-to-V-bit and inverse V-to-U-bit maps are generated to simplify, respectively, the computational complexity at the transmitter and receiver sites.

However, the traditional Lloyd algorithm is still very complex and time consuming. For example, in a 15-to-8-digit compression, the Lloyd algorithm needs to determine 256 (2^8) quantization levels and 257 thresholds through thousands of iterations, thus incurring a large number of

operations and a higher delay. To address such an issue, we demonstrated the R-Lloyd algorithm in Ref. [16], where the regular Lloyd algorithm is only used to determine the 2^P major quantization levels out of 2^V total number of levels in the first step. Then, $2^{(V-P)}$ minor quantization levels are uniformly interpolated within each quantization segment $[l_i \quad l_{i+1}]$. The selection of the number of major digits (P) and minor digits ($V-P$) needs to jointly consider the signal performance after compression and de-compression, as well as the computational complexity. The simulated EVM convergence of OFDM signals after 15-to-8-digit compression and de-compression processes when applying a different number of major digits are shown in Figs. 4(a)–4(d). It can be noted that there is a trade-off between the recovered signal quality and convergence speed. With fewer number of major digits, e.g., $P=3$, the algorithm converges quickly within 50 iterations but the EVM value is poorer. On the other hand, when increasing the number of major digits to $P=4$ or 5, the final EVM performance can be improved at the expense of slower convergence speed. Precisely, the results indicate that the signal quality is better, but the computational complexity is increased when increasing the major quantization levels rather than uniformly inserting the same number of minor quantization levels. However, when further enlarging the P value to $P=6$, the convergence speed is significantly reduced, thus seriously reducing the computing efficiency, and this may not work for low-latency MFH systems. Thus, to make a good balance between accuracy and complexity, 4 and 5 major digits are recommended. In this paper, five major digits with 500 iterations for 15-to-8-digit compressions are adopted.

The performance of EVM after recovering the compressed signal versus the number of quantization digits under different methods is shown in Fig. 5. In the simulation of compressing and de-compressing OFDM wireless signals as shown in Fig. 5(a), the 5G-NR-like data format [29] is applied where the subcarrier spacing is set to be

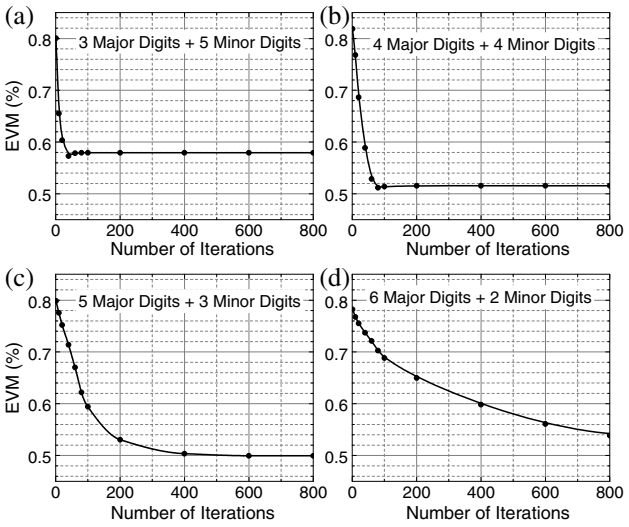

Fig. 4. EVM performance versus number of iterations when applying different numbers of major digits.

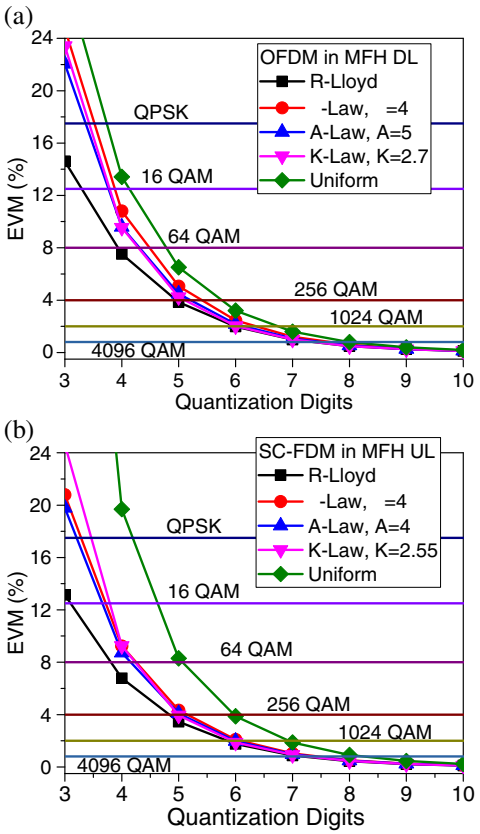

Fig. 5. EVM after de-compression versus number of digits using the wireless modulation formats of (a) OFDM and (b) SC-FDM.

$4 \times 15 = 60$ KHz; the total number of subcarriers is 2048, with 1201 subcarriers loaded with data. 16-QAM is adopted and each original OFDM I or Q sample calculated by a baseband processor is assumed to have 15 digits. The tested number of samples is 1,43,360, which covers 10 subframes of LTE signal. Five methods are compared here, including the R-Lloyd algorithm, μ-Law with $\mu=4$, A-Law with $A=5$, K-Law with $K=2.7$, and uniform PBS, which uniformly re-quantizes each sample from 15 digits to 3-to-10 digits. The coefficients of each method have been optimized. The EVM thresholds of 18.5%, 12.5%, 8%, and 4% are for QPSK, 16-QAM, 64-QAM, and 256-QAM, respectively, which are referred from 3GPP TS 36.104 [30] and 3GPP TS 36.872 [31], are marked on the figures. The EVM threshold of 1024-QAM is set at 2% taking reference from 3GPP TR 36.783 [32]. For 4096-QAM, the threshold is assumed to be 0.8%.

It can be observed that, among all the methods, R-Lloyd can obtain the best EVM performance after de-compression, especially for compressing to less than six digits. With four digits, the EVM can reach 7.56%, enough to pass the 64-QAM EVM threshold at the base station. With eight digits, the EVM can reach 0.49%, with a margin of more than 24 dB from the 64-QAM threshold. Other than OFDM as the LTE downlink (DL) format, the performance of SC-FDM in the LTE uplink (UL) is also evaluated as shown in Fig. 5(b). All the parameters are exactly the same as those in OFDM; the only difference arises because a

discrete-Fourier-transform spread operation is added before the IFFT. It can be seen that, compared with OFDM, the R-Lloyd algorithm shows good performance under SC-FDM. When compressed to 4 and 5 digits, EVMs of 6.78% and 3.46% are obtained, which pass, respectively, the 64-QAM and 256-QAM thresholds. It is also worth mentioning that the performance of the K-Law method for SC-FDM is degraded compared with that of OFDM. The penalty becomes larger especially with fewer number of quantization digits after compression. As mentioned before, because the signal amplitude of SC-FDM does not follow a Gaussian distribution, the performance of K-Law is expected to be weakened since it is based on a Gaussian PDF assumption. However, since R-Lloyd is based on an adaptive algorithm to fit the unique statistical properties of different waveforms, its performance is more stable and accurate than those of K-Law and non-adaptive traditional methods.

IV. Data Compression Enhanced by Adaptive Differential Pulse-Code Modulation

A. Linear Differentiator in Differential Pulse-Code Modulation With the Least-Mean-Square Algorithm

Aside from the quantizer design, another important technique to improve the compression ratio and bandwidth efficiency in D-RoF-based MFH is DPCM. In what follows, it can be seen that through weighted differential coding, the variance of the error function between the original and predicted samples can be reduced, thus resulting in an improved SQNR performance compared with that of regular PCM with the same number of quantization levels. Here, the SQNR can be calculated as

$$\mathrm{SQNR} = \frac{P_{\mathrm{signal}}}{P_{\mathrm{quantization\_noise}}} = \frac{E[|x(k)|^2]}{E[|x(k)-\hat{x}(k)|^2]}. \tag{9}$$

Since the bandwidth efficiency is dependent on the reduction of quantization digits, which is fundamentally rooted on the improvement of the SQNR, a higher bandwidth efficiency can be achieved in D-RoF-based MFH using a well-trained DPCM precoder to significantly suppress the quantization noise level. From Ref. [33], it has been proved that the SQNR improvement, I_s, can be approximated as

$$I_s = \frac{\mathrm{SQNR_{DPCM}}}{\mathrm{SQNR_{PCM}}} = \frac{\mathrm{Var}_s^2}{e_{\mathrm{MSE},D}^2}, \tag{10}$$

where Var_s^2 is the mean-square variance for the original samples, and $e_{\mathrm{MSE},D}^2$ is the MSE between the original and predicted samples, which is calculated as

$$e_{\mathrm{MSE},D}^2 = E[|x(k)-\hat{x}(k)|^2] = E[|\mathrm{err}(k)|^2], \tag{11}$$

where $x(k)$ is the kth sample of the original signal; $\hat{x}(k)$ is the predicted signal; and $\mathrm{err}(k)$ is the kth sample in the error signal calculated by the difference between $x(k)$ and $\hat{x}(k)$, same as Eq. (1). From Eq. (10), under a given original signal, a better SQNR is obtained after DPCM with a smaller mean-square variance of the error signal, which could be achieved by carefully calculating the tap coefficients shown in Eq. (2). Figures 6(a) and 6(b) compare, respectively, the waveform time-domain patterns and PDFs of the amplitudes between the error and original signals. Again, one 5G-NR-like OFDM signal with 2048 subcarriers and a bandwidth of 122.8 MHz is used here. Third-order DPCM with optimized weights is applied and it is observed that, after normalization, the variance of the error signal, which is one of the major contributors to the quantization noise, is significantly reduced from both the waveform patterns and PDFs. In what follows, methods to efficiently calculate the optimized tap values in the differential encoder will be discussed.

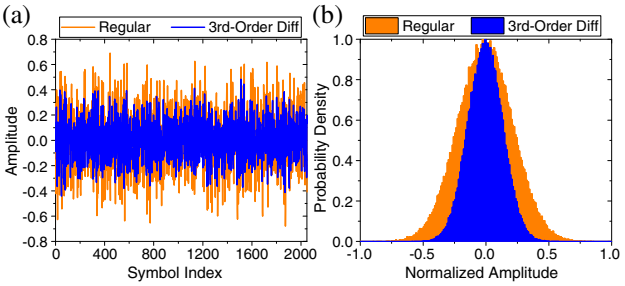

Fig. 6. (a) Amplitude and (b) probability density distribution of regular and third-order differentiated OFDM waveforms.

As demonstrated in the previous section, the objective of the DPCM encoder in data compression is to suppress the SQNR, which is realized by minimizing the MSE, $e_{\mathrm{MSE},D}^2$, through a linear prediction given in Eq. (2). Based on this concept, the architecture of a differentiator in DPCM is plotted in Fig. 7. The original baseband signal, $x(k)$, is linearly filtered by a multi-tap delay-line-based finite impulse response (FIR) filter to generate the predicted signal, $\hat{x}(k)$, before differentiating them to get the error signal, $\mathrm{err}(k)$. The weights of the FIR filter can be adaptively adjusted to reduce the MSE calculated by Eq. (11). It is worth noting that the objective and architecture of the system are very similar to those of the adaptive filter in the equalizer with the LMS algorithm for a digital communication system, which aims at minimizing the MSE between the received and transmitted signals. Thus, a similar iteration algorithm in a LMS-based equalizer can also be used to solve

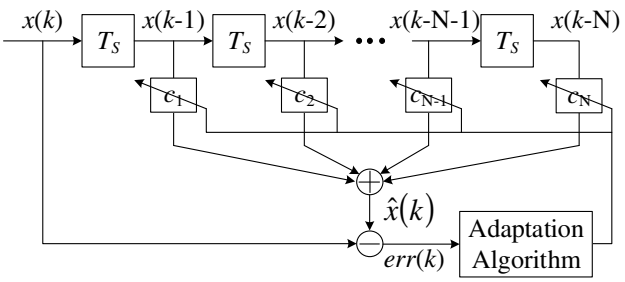

Fig. 7. Architecture of a LMS-based differentiator.

the weights of the delay taps in the differentiator. The weights are updated following the relations

$$\hat{x}(k) = \mathbf{c}(k) * \mathbf{v}(k), \tag{12}$$

$$\mathrm{err}(k) = x(k) - \hat{x}(k), \tag{13}$$

$$\mathbf{c}(k+1) = \mathbf{c}(k) + \mu \cdot \mathrm{err}(k) \cdot \mathrm{conj}[\mathbf{v}(k)], \tag{14}$$

where $\mathbf{v}(k) = [\ x(k-1) \quad x(k-2) \quad \ldots \quad x(k-N)\ ]^T$ is the input data vector; $\mathbf{c}(k) = [\ c_1(k) \quad c_2(k) \quad \ldots \quad c_N(k)\ ]$ is the FIR tap-weight vector; and μ is the step size. By properly setting the initial tap-weight vector and step size, the LMS algorithm can be made to quickly converge and provide a good approximation to the MMSE algorithm without calculating the inverse of the correlation matrix; this reduces the computational complexity especially for a high-order predictor. Another advantage of the LMS algorithm is that the system can keep updating the weights of the FIR filter adaptive to the real-time channel conditions; this could potentially benefit the wireless UL transmission with more bursty signals.

B. Data Compression in Mobile Fronthaul With Joint DPCM-NUQ Architecture

To further enhance the performance of the data compressor with a higher compression ratio, the differentiator and NUQ can work together in a feedback-loop-based system at the transmitter and receiver sites as shown in Fig. 8(a) and 8(b), respectively. When using the differentiator, the quantization noise generated from the quantizer will be transferred and accumulated from one symbol to another, thus degrading the quality of the recovered signal. Therefore, except from enabling the joint working of the quantizer and differentiator, another important purpose of the feedback loop is to resolve the issue of quantization noise transfer.

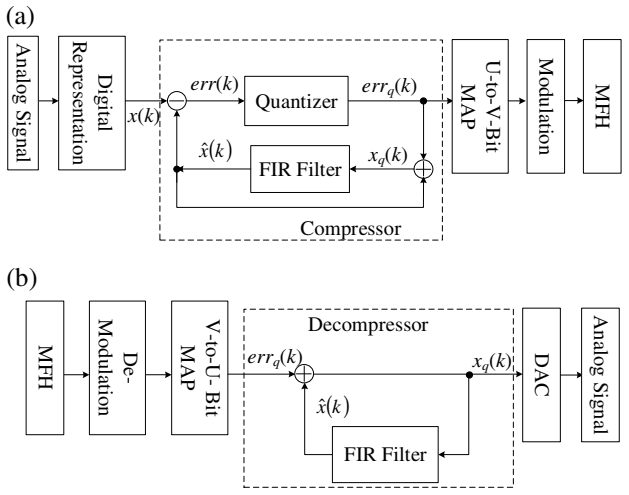

Fig. 8. Structures of (a) transmitter and (b) receiver with a joint DPCM-non-uniform-quantizer-based compressor in MFH.

For the data compressor at the transmitter site, in the kth iteration, the input error signal $\mathrm{err}(k)$, the quantized error signal $\mathrm{err}_q(k)$, and the quantized baseband signal $x_q(k)$ can be calculated, respectively, as

$$\mathrm{err}(k) = x(k) - \hat{x}(k) = x(k) - \sum_{i=1}^{N} c_i x_q(k-i), \tag{15}$$

$$\mathrm{err}_q(k) = \mathrm{err}(k) + n_q(k), \tag{16}$$

$$x_q(k) = \hat{x}(k) + \mathrm{err}_q(k) = \sum_{i=1}^{N} c_i x_q(k-i) + \mathrm{err}_q(k), \tag{17}$$

where $n_q(k)$ is the quantization noise at the kth sample, and $\hat{x}(k)$ is the output of the FIR filter, also known as the predictor of $x(k)$. From Eqs. (15) to (17), it can be deduced that

$$x_q(k) = x(k) + n_q(k). \tag{18}$$

It can be noted from Eq. (18) that the quantization noise from previous symbols is cancelled out and the quality of each quantized symbol is only determined by the current quantization noise. At the de-compressor at the receiver site, the baseband samples after quantization can be reconstructed using Eq. (17).

In the compression and de-compression processes, different NUQ algorithms can be used in the quantizer part, as shown in Fig. 8(a), to enhance its performance. In the following context of this paper, μ-Law, A-Law, K-Law, and R-Lloyd algorithms are applied and compared. To confirm the effectiveness of the LMS algorithm in the feedback-loop-based compressor architecture, comparisons are made between first- and second-order DPCM based on LMS and LUT. In the LUT method, a table is built with the EVM of the wireless signal measured as a function of tap coefficients. By searching all possible values in a given range, the combination of tap weights with a global optimization with the best EVM value can be figured out, when the step size is fine enough. The waveform under test is a 5G-NR OFDM signal with 2048 and 1201 total and loaded subcarriers, respectively. The waveform contains 1,43,360 samples covering 10 subframes. The EVM values given by the first- and second-order LUTs under 15-to-6-digit compression are plotted, respectively, in Figs. 9 and 10. In the first-order DPCM where $\hat{x}(k) = c_1 x_q(k-1)$, the change of EVM can be plotted as a one-dimensional curve. The tap weight and EVM obtained through LMS are also marked on the corresponding curve, where the tap weights are calculated through iterations from Eqs. (12) to (14). As shown in Fig. 9, it can be noted that the coefficient c_1 calculated by LMS is very close to the bottom of the curves, where the global optimal c_1 is obtained. Similarly, we compared the performance of the second-order DPCM-NUQ joint compressor between the LUT and LMS algorithms. In this case, $\hat{x}(k) = c_1 x_q(k-1) + c_2 x_q(k-2)$, and the EVM value is optimized by varying c_1 and c_2 in the LUT method as shown by the two-dimensional contour plots in Figs. 10(a)–10(d). The distributions applying different compression algorithms have similar shapes. The tap

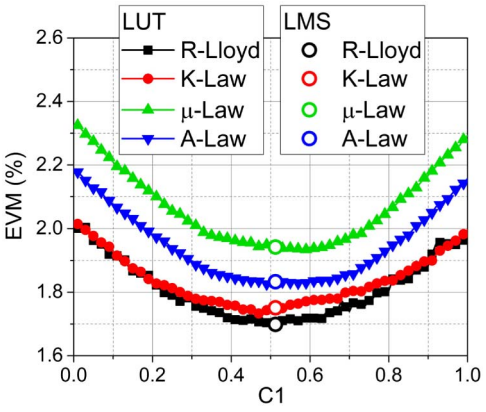

Fig. 9. EVM versus tap weights of the wireless signal after applying first-order DPCM combined with different quantization algorithms.

coefficients (c_1 and c_2) calculated by the LMS method are also marked on the figure. Their positions are quite close to the minimal points on the surface with the best EVM values, which proves that the result from LMS is a good approximation of the global optimized tap weights in a DPCM-NUQ joint architecture.

The performance of the proposed compressor adopting different companding algorithms is compared in Fig. 11 using PCM, first-order DPCM, and second-order DPCM. The

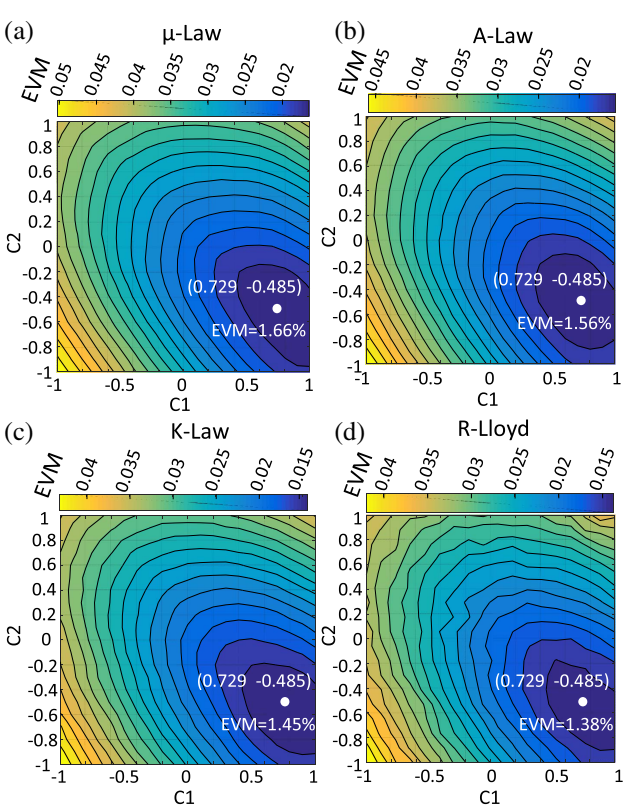

Fig. 10. EVM versus tap weights of the wireless signal after applying second-order DPCM combined with different quantization algorithms.

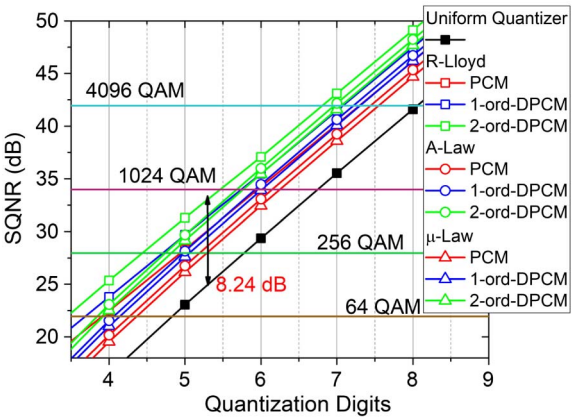

Fig. 11. SQNR versus quantization digits for compressors using PCM, first-order DPCM, and second-order DPCM with different NUQs.

SQNRs of the wireless baseband signal after compression and de-compression are measured here. On a decibel scale, all the curves are approximately linearly distributed as a function of the number of quantization digits. There is an improvement of around 6 dB in the SQNR upon adding one more quantization digit. Compared with PCM, the first- and second-order DPCMs can bring about extra SQNR improvements of 1.4 and 1.24 dB, respectively.

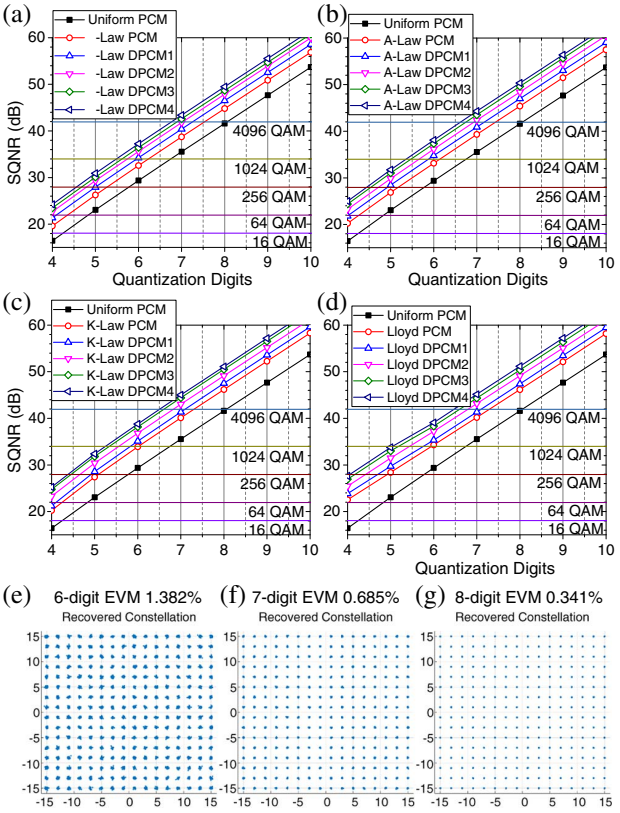

Fig. 12. (a)–(d) SQNR versus quantization digits under different orders of DPCM. (e)–(g) Selected constellations of recovered wireless signals with 256-QAM.

By combining second-order DPCM and the R-Lloyd algorithm, total SQNR improvement of 8.24 dB can be achieved. Considering SQNR improvement of nearly 6 dB can be traded into one quantization digit reduction, the joint DPCM-NUQ architecture is effective in improving the quantization efficiency.

The performance among different orders of DPCM when using μ-Law, A-Law, K-Law, and R-Lloyd are compared in Figs. 12(a)–12(d). It can be observed that the SQNR can be improved with an increase in the order of DPCM from 1 to 4, although the gain margin is also reduced. And considering the complexity introduced by the high-order DPCM, the first- to fourth-order DPCM schemes are recommended to be used here; in what follows, their performance in a MFH testbed have been studied. The SQNR thresholds of 16-QAM, 64-QAM, 256-QAM, 1024-QAM, and 4096-QAM in Figs. 12(a)–12(d) are estimated as 18.1, 21.938, 27.959, 33.98, and 41.94 dB, based on their EVM thresholds discussed before. As shown in Fig. 12(d), by jointly applying R-Lloyd and fourth-order DPCM, total SQNR improvement of around 10 dB can be obtained. Under 15-to-8-digit (quantization digits = 8) compression and de-compression, 51.15 dB SQNR can be achieved with nearly a 29 dB margin from 64-QAM SQNR threshold. The selected 256-QAM constellations with 6–8 quantization digits using the proposed fourth-order DPCM and R-Lloyd joint compressor and de-compressor are shown in Fig. 12(e)–12(g). EVM less than 1.4% is obtained, which is difficult to be achieved using traditional A-RoF systems for MFH data transmission.

V. Experimental Demonstrations

The capacity of future wireless systems can be significantly boosted through space-division multiplexing technologies, such as massive MIMO and small cell implementation. According to the latest 5G specifications [34], the peak data rate for DL could reach 20 Gbit/s, with up to 32 MIMO ports. On the other hand, the utilization of the 6–30 GHz band and extremely high-frequency bands beyond 30 GHz for future wireless broadband transmission attracts a lot of attentions [35–37]. To support the significantly increased wireless throughput following increased MIMO ports and higher-RF-band exploitation in 5G, coherent optics can be a good solution to provide sufficient fronthaul capacity, high receiver sensitivity, and large-scale connectivity.

In the former sections, we demonstrated the operation principles of different data-compression techniques in D-RoF-based MFH systems and compared their performance mainly based on simulations. In what follows, to demonstrate the feasibility of D-RoF-based coherent optical MFH, a point-to-point experimental testbed, as shown in Fig. 13, has been set up, where the robustness of the data-compression algorithm under the presence of bit errors is studied. The impacts of bit errors on the different combinations of compression algorithms in the coherent optical system have also been compared.

As shown in Fig. 13, in the coherent MFH, a dual-polarization IQ modulator (DP-IQM) is used as the

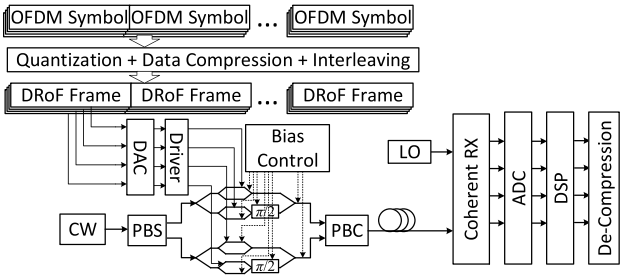

Fig. 13. Experimental system diagram.

transmitter at the CU site. The samples from wireless OFDM symbols are digitized and compressed to eight digits per sample. After digitization, each sample is converted into an 8 bit binary AxC chip. A CPRI-like data multiplexing scheme is utilized, where AxC chips from different antennas are interleaved to form D-RoF frames. Every two streams of data frames are mapped into QPSK or 16-QAM symbols offline, which are then sent to a 92 GSa/s arbitrary waveform generator and modulated onto the light in X or Y polarization through the DP-IQM. After transmission through 80-km single-mode fiber, the optical signal is received with a coherent detector and decomposed into four electrical signals captured by a four-channel real-time sampling oscilloscope operating at 80 GSa/s. The offline DSPs are applied to demodulate the coherent optical QPSK or 16-QAM signals. Then the D-RoF frames are recovered and after de-compression, they are used to reconstruct the wireless OFDM signals. In the optical part of the experiment, 36 Gbaud DP-QPSK and 32 Gbaud DP-16-QAM are tested, and their bit error rate (BER) performance as well as the selected constellations are shown in Fig. 14. Each OFDM wireless CC under test contains 2048 subcarriers and occupies a bandwidth of around 122.8 MHz. Out of the 2048 subcarriers, 1201 are loaded with 16-QAM symbols. For the coherent system with 32 Gbaud DP-16-QAM at a net information rate of 200 Gbit/s after excluding around 20% overhead for soft-decision FEC [38], 90 or 110 CCs can be encapsulated under 15-to-8-digit or 15-to-7-digit compression, respectively.

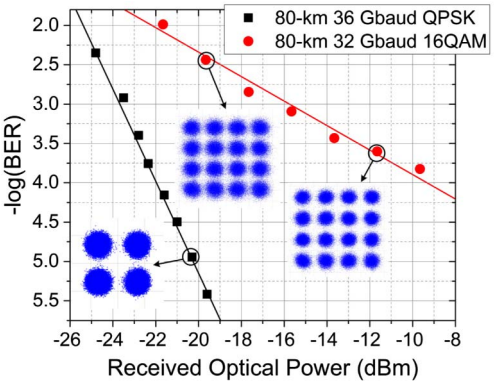

Fig. 14. BER versus the received optical power of the coherent MFH testbed.

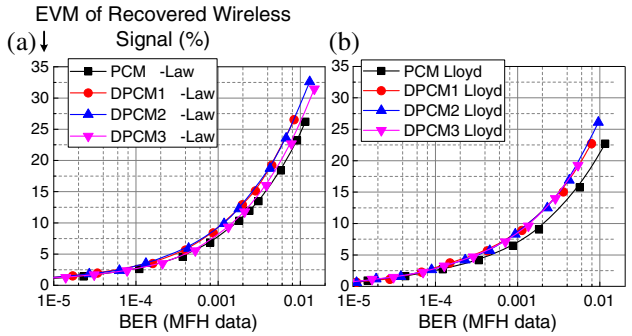

Fig. 15. EVM of the recovered wireless signal versus the BERs of the MFH data using (a) μ-Law DPCM and (b) Lloyd DPCM.

The EVM performance of the recovered wireless OFDM signal after the compression–decompression process, under the influence of bit errors in the MFH system, is shown in Fig. 15. It can be seen from Eq. (9) that, without FEC, bit errors further increase the deviations between $x(k)$ and $\hat{x}(k)$, thus degrading the SQNR. The compression methods of DPCM-μ-Law and DPCM-Lloyd have been compared in Fig. 15(a) and 15(b), respectively. In the cases of using DPCM-μ-Law and DPCM-Lloyd, less than 2% and 4% EVMs can be achieved with BER values smaller than 2×10^{-5} and 1×10^{-4}, respectively. It is worth noting that the BER performance of DPCM is slightly worse than that of regular PCM. Although the feedback-loop-based compressor architecture at the transmitter site can eliminate the issue of quantization-error accumulation in differential coding, the decision errors at the receiver site can still be transferred and accumulate from one sample to another in the decoding process of DPCM, thus degrading the BER performance of DPCM. However, the degradation is insignificant, and it can be mitigated by FEC where error-free performance can be achieved when the system can pass the threshold.

VI. Conclusion

In this work, multiple data-compression techniques have been investigated and implemented to improve the bandwidth efficiency of a next-generation D-RoF-based MFH system supporting 5G-NR. These include NUQ and DPCM. Based on our previous work discussing NUQ [16], more details and theoretical analysis on an R-Lloyd-algorithm-based compressor are provided. By varying the number of major and minor quantization levels, a good trade-off between quantization accuracy and computational complexity can be achieved. Meanwhile, R-Lloyd does not rely on the assumption of a Gaussian distribution and it can be adapted to different kinds of wireless signal formats. On the other hand, to further enhance the data compression ratio and system adaptability, a computationally efficient LMS algorithm is proposed to calculate the tap weights for a high-order DPCM encoder. After combining the NUQ and DPCM in a feedback-loop-based compressor, great improvements in SQNR can be obtained, thus leading to a good wireless signal quality after the compression and de-compression processes with fewer quantization digits. With fourth-order DPCM plus the R-Lloyd algorithm, SQNR improvement of 10 dB can be successfully achieved. EVM less than 0.4% and 0.7% can also be realized under 15-to-8-digit and 15-to-7-digit compressions, respectively. The proposed algorithms have been verified over a high-capacity MFH testbed based on coherent optics to support future mobile systems with massive MIMO or densified small cells. The encapsulated wireless signals can be recovered with EVM less than 0.8%. The influence of the measured bit errors in the optical MFH on the wireless signal quality has also been analyzed. According to the experimental results, the proposed approach for data compression has been validated as a promising solution to significantly improve the bandwidth efficiency for future D-RoF-based MFH supporting 5G.

References

[1] S. Y. Lien, S. L. Shieh, Y. Huang, B. Su, Y. L. Hsu, and H. Y. Wei, "5G New Radio: waveform, frame structure, multiple access, and initial access," *IEEE Commun. Mag.*, vol. 55, no. 6, pp. 64–71, 2017.

[2] "C-RAN: the road towards green RAN," China Mobile White Paper, 2011. Available: https://pdfs.semanticscholar.org/eaa3/ca62c9d5653e4f2318aed9ddb8992a505d3c.pdf

[3] "Study on new radio access technology: radio access architecture and interfaces (Release 14)," 3GPP TR 38.801, v14.0.0, 2017.

[4] C.-L. I, H. Li, J. Korhonen, J. Huang, and L. Han, "RAN revolution with NGFI (xhaul) for 5G," *J. Lightwave Technol.*, vol. 36, no. 2, pp. 541–550, 2018.

[5] X. Liu, F. Effenberger, N. Chand, L. Zhou, and H. Lin, "Demonstration of bandwidth-efficient mobile fronthaul enabling seamless aggregation of 36 E-UTRA-like wireless signals in a single 1.1-GHz wavelength channel," in *Optical Fiber Communication Conf. (OFC)*, Mar. 2015, paper M2J.2.

[6] X. Liu, H. Zeng, N. Chand, and F. Effenberger, "Experimental demonstration of high-throughput low-latency mobile fronthaul supporting 48 20-MHz LTE signals with 59-Gb/s CPRI-equivalent rate and 2-μs processing latency," in *European Conf. on Optical Communication (ECOC)*, Sept. 2015, paper We.4.4.3.

[7] M. Xu, J.-H. Yan, J. Zhang, F. Lu, J. Wang, L. Cheng, D. Guidotti, and G.-K. Chang, "Bidirectional fiber-wireless access technology for 5G mobile spectral aggregation and cell densification," *J. Opt. Commun. Netw.*, vol. 8, no. 12, pp. B104–B110, 2016.

[8] J. Wang, C. Liu, J. Zhang, M. Zhu, M. Xu, F. Lu, L. Cheng, and G.-K. Chang, "Nonlinear inter-band subcarrier intermodulations for multi-RAT OFDM wireless services in 5G heterogeneous mobile fronthaul networks," *J. Lightwave Technol.*, vol. 34, no. 17, pp. 4089–4103, 2016.

[9] J. Zhang, J. Wang, M. Xu, F. Lu, L. Chen, J. Yu, and G.-K. Chang, "Memory-polynomial digital pre-distortion for linearity improvement of directly-modulated multi-IF-over-fiber LTE mobile fronthaul," in *Optical Fiber Communication Conf. (OFC)*, Mar. 2016, paper TU2B.3.

[10] Q. Zhang, N. Stojanovic, C. Prodaniuc, F. Karinou, and C. Xie, "Cost-effective single-lane 112 Gb/s solution for mobile fronthaul and access applications," *Opt. Lett.*, vol. 41, no. 24, pp. 5720–5723, 2016.

[11] Qualcomm, "Accelerating the mobile ecosystem expansion in the 5G era with LTE Advanced Pro," Technical Presentation, 2018.

[12] A. de la Oliva, J. A. Hernandez, D. Larrabeiti, and A. Azcorra, "An overview of the CPRI specification and its application to C-RAN-based LTE scenarios," *IEEE Commun. Mag.*, vol. 54, no. 2, pp. 152–159, 2016.

[13] S. H. Kim, H. S. Chung, and S. M. Kim, "Experimental demonstration of CPRI data compression based on partial bit sampling for mobile front-haul link in C-RAN," in *Optical Fiber Communication Conf. (OFC)*, Mar. 2016, paper W1H.5.

[14] B. Guo, W. Cao, A. Tao, and D. Samardzija, "LTE/LTE-A signal compression on the CPRI interface," *Bell Labs Tech. J.*, vol. 18, no. 2, pp. 117–133, 2013.

[15] "Open radio equipment interface (ORI), ORI interface specification. Part 1: low layers (Release 4)," ETSI GS ORI 002-1, v4.1.1, 2014.

[16] M. Xu, Z. Jia, J. Wang, L. A. Campos, and G.-K. Chang, "A novel data-compression technology for digital mobile fronthaul with Lloyd algorithm and differential coding," in *Optical Fiber Communication Conf. (OFC)*, Mar. 2018, paper Tu2K.2.

[17] M. Xu, F. Lu, J. Wang, L. Cheng, D. Guidotti, and G.-K. Chang, "Key technologies for next-generation digital RoF mobile fronthaul with statistical data compression and multiband modulation," *J. Lightwave Technol.*, vol. 35, no. 17, pp. 3671–3679, 2017.

[18] L. Zhang, X. Pang, O. Ozolins, A. Udalcovs, S. Popov, S. Xiao, W. Hu, and J. Chen, "Spectrally efficient digitized radio-over-fiber system with k-means clustering-based multidimensional quantization," *Opt. Lett.*, vol. 43, no. 7, pp. 1546–1549, 2018.

[19] L. Zhang, X. Pang, O. Ozolins, A. Udalcovs, R. Schatz, U. Westergren, G. Jacobsen, S. Popov, L. Wosinska, S. Xiao, W. Hu, and J. Chen, "Digital mobile fronthaul employing differential pulse code modulation with suppressed quantization noise," *Opt. Express*, vol. 25, no. 25, pp. 31921–31936, 2017.

[20] Y. Yoshida, "Mobile Xhaul evolution: enabling tools for a flexible 5G Xhaul network," in *Optical Fiber Communication Conf. (OFC)*, Mar. 2018, paper Tu2K.1.

[21] "Common public radio interface: eCPRI interface specification," eCPRI Specification V1.0, 2017.

[22] D. Brubaker, W. Qian, M. Sussmann, Y. Takafuji, M. Akhter, and T. Hiatt, "The emerging need for fronthaul compression," Altera Corporation White Paper, June 2016, pp. 1–12. Available: https://www.intel.com/content/dam/www/programmable/us/en/pdfs/literature/wp/wp-01265-the-emerging-need-for-fronthaul-compression.pdf

[23] K. Miyamoto, S. Kuwano, T. Shimizu, J. Terada, and A. Otaka, "Performance evaluation of Ethernet-based mobile fronthaul and wireless comp in split-PHY processing," *J. Opt. Commun. Netw.*, vol. 9, no. 1, pp. A46–A54, 2017.

[24] M. Xu, X. Liu, N. Chand, F. Effenberger, and G.-K. Chang, "Fast statistical estimation in highly compressed digital RoF systems for efficient 5G wireless signal delivery," in *Optical Fiber Communication Conf. (OFC)*, Mar. 2017, paper M3E.7.

[25] H. Li, X. Li, and M. Luo, "Improving performance of differential pulse coding modulation based digital mobile fronthaul employing noise shaping," *Opt. Express*, vol. 26, no. 9, pp. 11407–11417, 2018.

[26] B. Farhang-Boroujeny, *Adaptive Filters: Theory and Applications*, 2nd ed. Wiley, 2013, Chap. 3.

[27] C. W. Brokish and M. Lewis, "A-Law and mu-Law companding implementations using the TMS320C54x," Texas Instruments Digital Processing Solutions, Appl. Note SPRA163A, Dec. 1997.

[28] P. Jardin and G. Baudoin, "Filter lookup table method for power amplifier linearization," *IEEE Trans. Veh. Technol.*, vol. 56, no. 3, pp. 1076–1087, 2007.

[29] S. Parkvall, E. Dahlman, A. Furuskar, and M. Frenne, "NR: the new 5G radio access technology," *IEEE Commun. Standards Mag.*, vol. 1, no. 4, pp. 24–30, 2017.

[30] "Base station (BS) radio transmission and reception (Release 12)," 3GPP TS 36.104, v12.10.0, 2016.

[31] "Small cell enhancements for E-UTRA and E-UTRAN: physical layer aspects (Release 12)," 3GPP TR 36.872, v12.1.0, 2013.

[32] "Introduction of 1024 quadrature amplitude modulation (QAM) in LTE downlink (Release 15)," 3GPP TR 36.783 v15.0.0, 2017.

[33] N. Benvenuto and G. Cherubini, *Algorithms for Communications Systems and their Applications*, 1st ed. Wiley, 2002, pp. 387–389.

[34] A. Ghosh, "5G New Radio (NR): physical layer overview and performance," in *IEEE Communication Theory Workshop*, May 2018, pp. 1–38.

[35] J. Yu, "Photonics-assisted millimeter-wave wireless communication," *IEEE J. Quantum Electron.*, vol. 53, no. 6, 8000517, 2017.

[36] X. Li, J. Yu, K. Wang, Y. Xu, L. Chen, L. Zhao, and W. Zhou, "Delivery of 54-Gbps 8QAM W-band signal and 32-Gbps 16QAM K-band signal over 20-km SMF-28 and 2500-m wireless distance," *J. Lightwave Technol.*, vol. 36, no. 1, pp. 50–56, 2018.

[37] X. Li, J. Yu, and J. Xiao, "Demonstration of ultra-capacity wireless signal delivery at W-band," *J. Lightwave Technol.*, vol. 34, no. 1, pp. 180–187, 2016.

[38] G. Tzimprogos, C. Kachris, I. B. Djordjevic, M. Cvijetic, D. Soudris, and I. Tomkos, "A survey on FEC codes for 100G and beyond optical networks," *IEEE Commun. Surveys Tuts.*, vol. 18, no. 1, pp. 209–221, 2016.